A dynamic hysteresis model of heat and mass transfer for hygrothermal bio-based materials

Yuliang Zou, Geoffrey Promis, Frédéric Grondin, Mazen Saad, Ahmed Loukili, Huan Wang

A dynamic hysteresis model of heat and mass transfer for hygrothermal bio-based materials

Yuliang Zou[a], Geoffrey Promis[b], Frédéric Grondin[c,*], Mazen Saad[d], Ahmed Loukili[c], Huan Wang[e]

[a]*Laboratoire Navier (Ecole des Ponts Paris Tech-Univ Gustave Eiffel-CNRS), 77420 Champs-sur-Marne, France*
[b]*Innovative Technologies Laboratory (LTI), University of Picardie Jules Verne, Avenue des Facultés—Le Bailly, CEDEX, 80025 Amiens, France*
[c]*Nantes Université, Ecole Centrale Nantes, CNRS, GeM, UMR 6183, F-44000 Nantes, France*
[d]*Laboratoire de Mathématiques Jean Leray (LMJL), CNRS UMR 6629, Centrale Nantes, 1 rue de la Noë, 44321 Nantes, France*
[e]*School of Highway, Chang'an University, 710064 Xi'an, China*

Abstract

The hygrothermal behaviour of porous building materials is significantly determined by the moisture and heat transfer phenomena. However, most of existing models used to predict this phenomenon neglect moisture hysteresis effect and dynamic capillarity effect, limiting their accuracy in assessing the efficiency and sustainability of bio-based building materials. To bridge this gap, the model presented in this paper considers both dynamic and hysteresis effects. The Finite Element Method (FEM) is adopted for the discrete approximation of the partial differential equations governing heat and moisture transfer. The model is validated with respect to experiment performed on bio-based material subjected to thermo-hygrical boundaries conditions. Results show unequivocally that dynamic capillarity effect and moisture hysteresis effect should be considered simultaneously to quantify hygrothermal behaviour of porous building materials. This critical insight underscores the significance of this research, offering a comprehensive model for evaluating the efficiency and sustainability of these materials by addressing the often-neglected aspects of moisture behaviour, i.e., dynamic and hysteresis effects. This model is marked by its precision and thorough consideration of essential factors, making it an indispensable contribution to the field and advances the understanding of the hygrothermal behaviour of bio-based building materials in real conditions. It would help in designing optimized building envelop.

Keywords: Dynamic effect, Hysteresis effect, Mathematical models, Moisture transport, Porous bio-based materials

Highlights

- Enhanced prediction of hygrothermal behaviour in bio-based building materials.
- Modelling the coupling of moisture hysteresis effects with dynamic capillary pressure.

*Corresponding author. Tel.: +33 (0) 2 40 37 16 68
Email addresses: yuliang.zou@univ-eiffel.fr (Yuliang Zou), geoffrey.promis@u-picardie.fr (Geoffrey Promis), Frederic.Grondin@ec-nantes.fr (Frédéric Grondin), mazen.saad@ec-nantes.fr (Mazen Saad), ahmed.loukili@ec-nantes.fr (Ahmed Loukili), wanghuan07@chd.edu.cn (Huan Wang)

- Advances understanding and aids building material design and optimization.

Nomenclature

τ	dynamic effect coefficient
P_v^{dyn}	dynamic vapour pressure
β	moisture transfer coefficient
δt_n	time increment
$\mathbf{\Phi}$	nodal value vectors of RH
$\mathbf{T}$	nodal value vectors of temperature
ϕ	relative humidity (RH)
$c_{p,l}$	heat capacity of liquid water
$c_{p,m}$	heat capacity of dry building materials
D_l	liquid transport coefficient
h	heat exchange coefficient
J_l	liquid water flux
J_v	water vapour flux
K	liquid water permeability
k	sorption curve fitting parameter
P_c	capillary pressure
P_c^{dyn}	dynamic capillary pressure
$P_v^{sat}(T)$	saturated vapour pressure
q	heat conduction
R	universal gas constant
T	absolute temperature
w	moisture content
δ_p	vapour diffusivity
C_G	sorption curve fitting parameter
$D_{l,\phi}$	liquid diffusion coefficient
$D_{l,ws}$	capillary transport coefficient
G_Ω	mass flux at open surfaces
h_{lv}	latent heat of evaporation
Q_Ω	heat flux at open surfaces
S_{ads}	saturation of main adsorption curve
S_{des}	saturation of main desorption curve
u	vapour diffusion resistance coefficient
w_m	monomolecular moisture content
δ_a	water vapour permeability of air
$\mathbf{N}^\phi$	RH shape function matrices
$\mathbf{N}^T$	temperature shape function matrices
ρ_m	dry porous material density
ρ_w	liquid water density
ξ_ϕ	moisture capacity
A_c	water absorption coefficient
$c_{p,m}$	dry material capacity
h_l	liquid water enthalpy
h_m	enthalpy of drying building materials
h_v	water vapour enthalpy
M_w	water molar mass
P_c	capillary pressure
P_v	vapour pressure
W_f	moisture content at free saturation
w_l	liquid moisture content
w_v	vapour moisture content

1. Introduction

New standards suggest to use more bio-based concrete in building construction in order to meet the increasing requirements on environment protection and cost limitation. Most of studies reveal that bio-based porous materials have high thermal performances and could regulate the indoor humidity levels [1–3]. Buildings exposed to natural environment always suffer periodic temperature and relative humidity. The heat and moisture transfer occurs simultaneously within building materials and results in a significant impact on the energy performance of buildings.

Plenty of models and formulas were established to specify the coupled heat and moisture transfer since the pioneering work of Philip and De Vries [4]. They developed a theory of moisture transport in porous materials under temperature gradients with the consideration of interaction of vapour, liquid and solid phases. Subsequently, a model capable of simulating under both isothermal and non-isothermal conditions was given by Luikov [5] on the basis of thermodynamics of irreversible processes. After that, models dedicated to building materials were developed in succession [6–10]. A typical model which adopts the relative humidity instead of water content as moisture driving potential was developed by Kunzel [9]. Various models and approaches showed that hygrothermal transfers in porous materials can be simulated by a darciean water flow, fickean vapour diffusion, heat conduction and enthalpy flow.

However, numerous approximations are made using first order approaches in mechanical formula. In order to perform transfer phenomenon according to documented models, the water vapour sorption isotherms (WVSIs) which describe moisture storage capacity are indispensible. Most of modellings are based on main or average water vapour sorption isotherms [6, 11–15]. Actually, the moisture storage function is greatly dependent on the previous state of water content, and there is a discrepancy between adsorption and desorption for water vapour sorption isotherms [16–20]. This phenomenon, supposed to be caused by ink-bottle effect, the variation of liquid-solid contact angle, pore-size distribution as well as pore connectivity, is known as moisture hysteresis effect [17, 21]. Even if models provide numerical results that have a higher agreement with experimental measurements (under certain conditions), visible discrepancy still exists. Particularly in the case of a fast variation of the ambient relative humidity.

Indeed, the fast change rate of relative humidity is not considered in classical models based on a first approach of fluid flow equations. It was observed that the water retention curve, measured under dynamic conditions, deviates from the static one [22]. Regarding the Laplace's equation, the pressure difference between gas mixture and liquid water in porous materials under dynamic conditions differs from the static equilibrium capillary pressure. This phenomenon is known as dynamic effect on capillary pressure. Analogous to water retention curve, the water vapour sorption isotherms of porous building materials is influenced by the dynamic capillarity effect [23]. Unlike the hysteresis effect, the dynamic effect is mainly due to the fast flow of fluid. In this case, the viscous forces become strong and require a supplementary pressure gradient to overcome [24–26]. The fundamental mechanisms of dynamic effect includes dynamic contact angles [27, 28], dynamic fluid spatial distribution [29, 30], dynamic interface deformation [28], and the effects of averaging homogeneous/heterogeneous flow [31, 32]. Recently, much attention has been paid to dynamic effect on unsaturated water-air flow in porous media with high permeability, such as soil and sand. However, very few publications in the literature consider the contribution of dynamic capillarity effect on moisture transport within hygroscopic building materials with relative low permeability.

This study aims to build a more complete heat and moisture transfer model with the consideration of dynamic capillarity effect and hysteresis effect for porous building materials subjected to periodic change of temperature and relative humidity. By addressing the often-neglected aspects of moisture behavior, this study contributes significantly to the understanding of hygrothermal behaviour of bio-based building materials and provides a valuable approach to modeling for architects, engineers, and material scientists working to improve building materials' performance. In this paper, three models were studied and compared:

- the 'dynamic hysteresis model' considers dynamic effect and hysteresis effect;
- 'hysteresis model' takes into account hysteresis effect and ignores the dynamic effect;
- 'standard model' considers neither dynamic effect nor hysteresis effect.

First of all, the specific derivation of dynamic hysteresis model is introduced. Thereafter, a documented experiment investigating hygrothermal behaviour of Date Palme Concrete (DPC) wall

is employed to verify the performance of the proposed model. Numerical results simulated by these three models are presented and compared with corresponding experimental data. The potential contribution of dynamic effect and hysteresis effect on heat and moisture transfer is discussed according to this comparison.

2. Dynamic physical model for moisture and heat transfer

Moisture and heat transfer models were developed on the basis of the mass conservation principle and energy conservation law, respectively. The following classical assumptions were adopted:

- The porous material was assumed to be homogeneous and isotropic. The impact of skeleton deformation and closed pores on heat and moisture transfer was totally neglected.
- A local thermodynamic equilibrium was assumed between porous skeleton, water and air. The liquid water remains incompressible.

2.1. Moisture transport model

The governing model for moisture transport is derived from the mass conservation principle of unsaturated water-air flow in porous materials. Considering that the density of gaseous phases is relative small compared with water density and the contribution of dry air on mass transport is weak, the mass conservation equations for liquid water and water vapour reduce to a simplified equation regarding moisture, i.e. including liquid water (l) and water vapour (v) [33]:

$$\frac{\partial w}{\partial t} + \nabla \cdot (J_l + J_v) = 0 \tag{1}$$

where w, J_l and J_v represent, respectively, the moisture content, the liquid water flux and the water vapour flux. As for weakly permeable porous materials, the moisture transport is greatly dependent on liquid water advection and water vapour diffusion. Because the gas pressure in pore is always assumed to be constant and equals to the atmospheric pressure, the contribution of water vapour advection is negligible.

The drive potential for the liquid water advection is the capillary pressure gradient [34]. The specific J_l is given by the extended Darcy's law:

$$J_l = -K\nabla\left(-P_c\right) \tag{2}$$

where K represents the liquid water permeability and P_c the capillary pressure. On the other hand, the drive force for the water vapour diffusion is density gradient. Because of the air mixture could be considered as ideal gas, J_v is provided according to Fick's law:

$$J_v = -\delta_p \nabla P_v \tag{3}$$

where δ_p represents the vapour diffusivity and P_v the vapour pressure.

Substitution of the extended Darcy's law (2) and Fick's law (3) into the simplified mass conservation equation (1) results in the following typical moisture transport model [34]:

$$\frac{\partial w}{\partial t} + \nabla \cdot \left(-K\nabla(-P_c) - \delta_p \nabla P_v\right) = 0 \tag{4}$$

In the case of a satisfied equilibrium between liquid water and water vapour, the Kelvin's equation provides the capillary pressure as a function of the relative humidity:

$$P_c = -\frac{\rho_w RT}{M_w} \ln \phi \tag{5}$$

where R represents the universal gas constant, T the absolute temperature, M_w the water molar mass and ρ_w the liquid water density. ϕ is the relative humidity given by $\phi = \frac{P_v}{P_v^{sat}(T)}$ were $P_v^{sat}(T)$ represents the saturated vapour pressure which is a temperature-dependant function [35]:

$$P_v^{sat}\left(T\right) = 610.7 \times 10^{7.5\times \frac{T-273.15}{T-35.85}} \tag{6}$$

In addition, the adsorption and desorption curves provide the constitutive relationship between

relative humidity and moisture content during the main wetting and drying processes of a given porous material. It indicates that the relationship between capillary pressure and moisture content can be derived from the sorption curves according to the Kelvin's equation. Moreover, all variables, including capillary pressure, vapour pressure, and moisture content, can be expressed as a function of relative humidity. Furthermore, by taking into account the impact of temperature on vapour pressure, the previous equation (4) transforms into the standard coupled model for moisture transport, in which the variables are relative humidity ϕ and temperature T:

$$\xi_\phi \frac{\partial \phi}{\partial t} + \nabla \cdot \left(-D_l \xi_\phi \nabla \phi - \delta_p \nabla \left(\phi P_v^{sat}(T) \right) \right) = 0 \tag{7}$$

where $\xi_\phi = \frac{\partial w}{\partial \phi}$ is the moisture capacity and $D_l = -K \frac{\partial P_c}{\partial w}$ is the liquid transport coefficient.

D_l consists of the liquid diffusion coefficient $D_{l,\phi}$ and the capillary transport coefficient $D_{l,ws}$. In the case of a high relative humidity:

$$D_{l,\phi} = \frac{P_v^{sat} \delta_a}{\xi_\phi} \left(\frac{1}{u^*(\phi)} - \frac{1}{u} \right) \tag{8}$$

where δ_a represents the water vapour permeability of air, u the vapour diffusion resistance coefficient at the beginning of capillary condensation and $u^*(\phi)$ the vapour diffusion resistance coefficient depending on the relative humidity. As for DPC materials, the vapour diffusion resistance coefficients u and $u^*(\phi)$ are measured by using dry and wet cup tests, respectively [19]. As for suction process in capillary region, the capillary transport coefficient is dependent on moisture content and given by the following expression [36]:

$$D_{l,ws} = \left(3.8 \left(\frac{A_c}{W_f} \right)^2 \cdot 1000^{\frac{w}{W_f} - 1} \right) \tag{9}$$

where A_c represents the water absorption coefficient and W_f the moisture content at free saturation.

2.2. Dynamic moisture transport model

The standard coupled model (Eq. 7) could be improved with the consideration of dynamic effect for the modelling of drying under low relative humidity. As suggested in typical moisture transport model, the time change rate of moisture content is determined by the divergence of the capillary pressure and the water vapour pressure.

On the basis of thermodynamic theories and constitutive conservation laws, the well-accepted equation (10) was proposed in [25] to establish the relationship between the actual (dynamic) capillary pressure (P_c^{dyn}) and the static capillary pressure:

$$P_c^{dyn} - P_c = -\tau \frac{\partial S_w}{\partial t} \tag{10}$$

where τ represents the dynamic effect coefficient, which determines the magnitude of dynamic capillarity effect.

On the other hand, the dynamic water vapour pressure is accessible due to a latent relation between capillary pressure and water vapour pressure provided by the Kelvin's equation (5). By considering dynamic effect, the Kelvin's equation (5) evolves to:

$$P_c^{dyn} = -\frac{\rho_w RT}{M_w} \ln \frac{P_v^{dyn}}{P_{vs}} \tag{11}$$

where P_v^{dyn} represents the dynamic vapour pressure. Thereafter, the dynamic Kelvin's equation minus the standard Kelvin's equation gives the relationship between dynamic and standard vapour pressure:

$$P_v^{dyn} = P_v \cdot e^{\left(\tau \frac{\partial S_w}{\partial t} \cdot \frac{M_w}{\rho_w RT}\right)} \tag{12}$$

Practically, equations (10) and (12) encompass the dynamic effect on water advection and vapour diffusion. By submitting these relations to replace the originally corresponding relations in the typical model (4), the preliminary dynamic model for moisture transport is given as follows:

$$\frac{\partial w}{\partial t} + \nabla \cdot \left(K \nabla \left(P_c - \tau \frac{\partial S_w}{\partial t} \right) - \delta_p \nabla \left(P_v \beta \right) \right) = 0 \tag{13}$$

where $\beta = e^{\left(\tau \frac{\partial S_w}{\partial t} \cdot \frac{M_w}{\rho_w RT}\right)}$. The additional terms of the above equation compared with the standard model indicate the auxiliary contribution on moisture transport caused by dynamic effect. The first one ($\tau \frac{\partial S_w}{\partial t}$) among them reveal the additional contribution of dynamic effect on water advection. The second one (β) corresponds to the additional contribution of dynamic effect on vapour diffusion.

In order to ensure efficient implementation of numerical process, the above governing equation for moisture transport is transformed to the following equation:

$$\begin{aligned} &\xi_\phi \dot{\phi} + \nabla \cdot \left(\left(K \frac{\partial P_c}{\partial w} \frac{\partial w}{\partial \phi} - \delta_p \beta P_v^{sat}(T) \right) \nabla \phi \right) \\ &\quad - \nabla \cdot \left(\left(K + \delta_p \phi P_v^{sat}(T) \frac{M_w \beta}{\rho_w RT} \right) \nabla \left(\xi_{dyn} \dot{\phi} \right) \right) \\ &\quad + \nabla \cdot \left(\left(\delta_p \phi P_v^{sat}(T) \frac{\xi_{dyn} \dot{\phi} M_w \beta}{\rho_w RT^2} - \delta_p \phi \beta \frac{\partial P_v^{sat}(T)}{\partial T} \right) \nabla T \right) = 0 \end{aligned} \tag{14}$$

where $\xi_\phi = \frac{\partial w}{\partial \phi}$, $\xi_{dyn} = \tau \frac{\partial S_w}{\partial \phi}$ and the superposed dot over ϕ denotes a time derivative.

2.3. Heat transfer model

The heat transfer in porous materials must follow the energy conservation law. In the case of moisture and heat transfer in porous materials, it means that the change of enthalpy in the controlled element is equal to the energy flow into the controlled element including heat conduction and enthalpy flow caused by moisture transport. The specific governing equation for heat transfer is given as follows:

$$\frac{\partial}{\partial t} \left(\rho_m c_{p,m} T + h_v w_v + h_l w_l \right) = \nabla \cdot \left(-q - h_v J_v - h_l J_l \right) \tag{15}$$

where ρ_m, $c_{p,m}$, w_v, w_l, q, h_v, h_l and h_{lv} represent, respectively, the density of the dry porous material, the specific capacity of the dry material, the vapour moisture content, the liquid moisture content, the heat conduction, the enthalpy of the water vapour, the enthalpy of the liquid water

and the latent heat of evaporation. The three last parameters are linked as follows:

$$h_v = h_l + h_{lv} \tag{16}$$

Substituting relation $w = w_l + w_v$ and (1) into the original heat transfer model (15) and assuming that the specific heat capacity of dry building materials $c_{p,m}$, heat capacity of liquid water $c_{p,l}$ and latent heat of evapouration h_{lv} are constant yield a standard model for heat transfer in porous materials:

$$\left(\rho_m c_{p,m} + w c_{p,l}\right) \frac{\partial T}{\partial t} = -\nabla \cdot (q + h_{lv} J_v) - (J_v + J_l)\, c_{p,l} \nabla T - h_{lv} \frac{\partial w_v}{\partial t} \tag{17}$$

where $c_{p,m} = \frac{\partial h_m}{\partial T}$ and $c_{p,l} = \frac{\partial h_l}{\partial T}$. h_m is the enthalpy of drying building materials.

Furthermore, compared with the latent heat of vapourization, the contribution of sensible heat of moisture on heat flow is negligible. In addition, even though the latent heat of vapourization is relatively large, an absolutely small time change rate of vapour content $\frac{\partial w_v}{\partial t}$ caused by long-term vapour transfer results in a negligible value for the product of h_{lv} and $\frac{\partial w_v}{\partial t}$ [37]. Therefore, the last two terms in (17) can be ignored. Considering that the heat conduction is dependent on temperature gradient and thermal conductivity λ, i.e. $q = -\lambda \nabla T$, and the water vapour flux is determined by vapour pressure gradient, i.e. $J_v = -\delta_p \nabla \left(\phi P_v^{sat}(T)\right)$, the convection equation of heat transfer transforms to a time evolution of temperature and relative humidity model:

$$\left(\rho_m c_{p,m} + w c_{p,l}\right) \frac{\partial T}{\partial t} = \nabla \cdot (\lambda \nabla T) + h_{lv} \nabla \cdot \left(\delta_p \nabla \left(\phi P_v^{sat}(T)\right)\right) \tag{18}$$

2.4. Dynamic heat transfer model

As the heat transfer is impacted by water vapour flux, the dynamic effect should also be considered in the heat transfer model. Analogous to the derivation of dynamic moisture transport model, by replacing dynamic water vapour pressure P_v^{dyn} to simplified energy conservation equation (18) to replace the initial static P_v, it leads to the dynamic model for heat transfer:

$$\left(\rho_m c_{p,m} + w c_{p,l}\right) \frac{\partial T}{\partial t} = \nabla \cdot (\lambda \nabla T) + h_{lv} \nabla \cdot \left(\delta_p \beta \nabla \left(\phi P_v^{sat}(T)\right) + \delta_p \phi P_v^{sat}(T) \nabla \beta\right) \tag{19}$$

The additional term β compared with initial typical model suggests the contribution of dynamic effect on heat transfer. In order to make the system amenable to efficient numerical treatment, the above dynamic model for heat transfer was modified to the following form:

$$\begin{aligned}
&\xi_T \dot{T} - \nabla \cdot (\lambda \nabla T) - h_{lv} \nabla \cdot \left(\delta_p \beta P_v^{sat}(T) \nabla \phi \right) \\
&\quad + h_{lv} \nabla \cdot \left(\left(\frac{\delta_p \phi P_v^{sat}(T) \xi_{dyn} \dot{\phi} M_w \beta}{T^2 \rho_w R} - \delta_p \beta \phi \frac{\partial P_v^{sat}(T)}{\partial T} \right) \nabla T \right) \\
&\quad - h_{lv} \nabla \cdot \left(\frac{\delta_p \phi P_v^{sat}(T) M_w \beta}{\rho_w R T} \nabla \left(\xi_{dyn} \dot{\phi} \right) \right) = 0
\end{aligned} \tag{20}$$

where $\xi_T = \rho_m C_{p,m} + w C_{p,l}$ and $\dot{T} = \frac{\partial T}{\partial t}$.

2.5. Hysteresis model of sorption isotherm

The constitutive relationship between relative humidity ϕ and moisture content w is indispensable to solve the coupled governing equation. Various models, such as Langmuir, BET, Van Genuchten and Guggenheim-Anderson-de Boer (GAB) models, have been developed in previous literature to define this relationship. Among existing models, the GAB model is often used for describing hygroscopic behaviour of a bio-based material over the entire relative humidity range:

$$w = \frac{w_m C_G k \phi}{(1 - k\phi)(1 - k\phi + C_G k \phi)} \tag{21}$$

where w_m represents the monomolecular moisture content and k and C_G are fitting parameters determined by latent heat of condensation and molar heat of absorption, respectively.

Significant hysteresis phenomenon between adsorption and desorption is a characteristic feature of the bio-based materials, especially in the relative humidity range of 25% to 75%. Different physics phenomena could explain this observation: ink-bottle effect, variation of liquid-solid contact angle, pore-size distribution and pore connectivity [38].

Until now, plenty of models have been built to implement hysteresis effect: the empirical model

of Pedersen [18], the conceptual model of Preisach [38], the thermodynamic model of Merakeb [39] and the phenomenological model of Mualem [40–42], etc. In this paper, the model Mualem II [40] was used. This model is based on two basic pore water distribution functions L and H, in which the argument is the capillary pressure:

$$L\left(P_c\right) = S_{ads}\left(P_c\right) \tag{22}$$

$$H\left(P_c\right) = \frac{S_{des}\left(P_c\right) - S_{ads}\left(P_c\right)}{1 - S_{ads}\left(P_c\right)} \tag{23}$$

where S_{ads} and S_{des} represent the saturation of the main adsorption curve and the saturation of the main desorption curve, respectively. The first wetting scanning curve starting on the main desorption curve at the point $\left(S_{ads}\left(P_c\right), P_{c,1}\right)$ is written as follows:

$$S_{ads}\left(P_c\right) = S_{des}\left(P_{c,1}\right) + \left[L\left(P_c\right) - L\left(P_{c,1}\right)\right] H\left(P_{c,1}\right) \tag{24}$$

After Nth wetting and drying switch, the expression for drying scanning curve of order $(N+1)$ is given as follows:

$$S_{des}\left(P_c\right) = S_{ads}\left(P_{c,N}\right) - \left[L\left(P_{c,N}\right) - L\left(P_c\right)\right] \cdot \left[1 - H\left(P_c\right)\right] \;\; for \; L\left(P_c\right) \geq L\left(P_{c,N-1}\right) \tag{25}$$

In the same manner, if water saturation increases after the reversal point after a certain number of drying and wetting cycles, the adsorption scanning curve is obtained by the following expression:

$$S_{ads}\left(P_c\right) = S_{des}\left(P_{c,N}\right) + \left[L\left(P_c\right) - L\left(P_{c,N}\right)\right] \cdot \left[1 - H\left(P_{c,N}\right)\right] \;\; for \; L\left(P_c\right) \leq L\left(P_{c,N-1}\right) \tag{26}$$

where $P_{c,N}$, $S_{ads}\left(P_{c,N}\right)$, $S_{des}\left(P_{c,N}\right)$ and $L\left(P_{c,N}\right)$ are values at the beginning point of the current scanning curve. $L\left(P_{c,N-1}\right)$ represents the value at the starting point of the previous scanning curve.

It must be emphasized that if $L\left(P_c\right) \leq L\left(P_{c,N-1}\right)$ for drying scanning curve calculation, $L\left(P_{c,N-3}\right)$ should be used to take the place of $L\left(P_{c,N-1}\right)$. Analogously, in the case of wetting, if

$L(P_c) \geq L\left(P_{c,N-1}\right)$, $L\left(P_{c,N-3}\right)$ is adopted instead of $L\left(P_{c,N-1}\right)$ for calculating wetting scanning curve. In another words, in order to implement Mualem's model accurately, it is vital to keep a record of the history of scanning curve.

In this paper, an incremental calculation method based on successive time step was adopted to calculate the scanning curve. The specific mathematical series for wetting scanning curve and drying scanning curve are written as following equations (27) and (28), respectively:

$$S_t - S_{t-1} = \left[L\left(P_{c,t}\right) - L\left(P_{c,t-1}\right)\right] + H\left(P_{c,1}\right) \cdot \left[L\left(P_{c,t-1}\right) - L\left(P_{c,t}\right)\right] \tag{27}$$

$$\begin{aligned} S_t - S_{t-1} =& L\left(P_{c,t}\right) \cdot \left[1 - H\left(P_{c,t}\right)\right] \\ & - L\left(P_{c,t-1}\right) \cdot \left[1 - H\left(P_{c,t-1}\right)\right] + L\left(P_{c,1}\right) \cdot \left[H\left(P_{c,t}\right) - H\left(P_{c,t-1}\right)\right] \end{aligned} \tag{28}$$

where $L\left(P_{c,1}\right)$ and $H\left(P_{c,1}\right)$ are values at the beginning point of adsorption or desorption cycle.

In order to incorporate the hysteresis model to simulate wetting and drying cycles, two issues must be solved. The first one is to check the reversal point. The second one is to identify the current state. The reversal point can be detected by establishing a mathematical function for time change of vapour concentration dc_v/dt at two adjacent time steps:

$$\left.\frac{dc_v}{dt}\right|_{t-1} \cdot \left.\frac{dc_v}{dt}\right|_{t} \tag{29}$$

On the condition of Eq. (29) > 0, there is no reversal point and the wetting or drying scanning curve continues. On the other hand, if Eq. (29) < 0, the scanning curve is switching. Furthermore, the wetting or drying scanning curve can be identified via the value of second derivative of vapour concentration d^2c_v/dt^2 . The positive value of d^2c_v/dt^2 indicates wetting scanning curve while drying scanning curve is reached for a negative value of d^2c_v/dt^2 .

The originality of our model lies in its ability to capture the coupled heat and mass transport phenomena, considering the complex interactions between temperature and relative humidity. Unlike conventional models, our proposed model incorporates dynamic effect terms and accounts for the hysteresis of sorption curve.

3. Presentation of the experimental test and numerical simulation

The main objective of this study was the assessment of the performance of the dynamic hysteresis model for the simulation of the behaviour of bio-based materials under varying thermo-hygrical boundary conditions. To achieve this, a comparison was performed between the modeling results obtained from the dynamic hysteresis model and documented experimental data available in the literature. This comparative analysis has been specifically focused on temperature and relative humidity distribution and their temporal evolution within the bio-based materials. FEM has been employed for obtaining quantitative solutions of the model.

3.1. Experimental tests

An experiment has been investigated by [43] to characterize the hygrothermal behaviour of Date Palme Concrete (DPC). Various scenarios were performed involving variation/cycling of temperature or relative humidity. This experiment serves as an appropriate example for validating the proposed dynamic and hysteresis model. The specific properties of DPC are summarized in Table 1. The data related to the relative humidity and moisture content relationship (RH-w) are collected from experimental measurement and fitted using the GAB model to determine the parameters w_m, C_G and k for adsorption and desorption, respectively. The fitting curve is shown is Fig.1 and the corresponding parameter values are presented in Table 2.

Table 1: Properties of DPC

Property	Value
Dry density	954 $\left(kg \cdot m^{-3}\right)$
Dry thermal conductivity	0.185 $\left(W \cdot m^{-1} \cdot K^{-1}\right)$
Dry specific heat	1500 $\left(J \cdot kg^{-1} \cdot K^{-1}\right)$
Moisture supplement of thermal conductivity	10.190 $(-)$
vapour resistance coefficient (dry cup)	6.310 $(-)$
vapour resistance coefficient (wet cup)	5.570 $(-)$
Water absorption coefficient	0.165 $\left(kg \cdot m^{-2} \cdot s^{-0.5}\right)$
Water content at free saturation	429 $\left(kg \cdot m^{-3}\right)$

Cuboid specimens were prepared to monitor the evolution of relative humidity and temperature at different depths. After three weeks of hardening, specimens extracted from the mold were placed

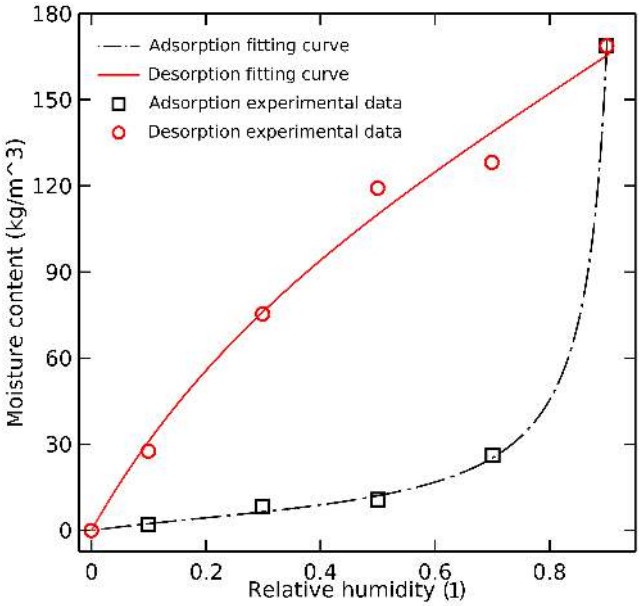

Figure 1: Sorption isotherms of DPC at 23 °C.

Table 2: Fitting parameters of GAB for adsorption and desorption isotherms

Parameter	Value	
	Adsorption	Desorption
w_m	7.0348	178.1118
C_G	3.6000	7.3320
k	1.0650	0.2707

in a controlled laboratory environment, maintained at a relative humidity of 50% and a temperature of $T = 20°C$, over a period of one year. This procedure ensures that the moisture content of first stage aligns with the desorption curve. The dimension of DPC wall were $50 \times 40 \times 15$ cm^3. The lateral surfaces of all studied specimens have been sealed with insulated polystyrene panels covered by a thin plastic film. In this way, 1D heat and moisture transfer across the thickness of the wall is imposed. The outside surface of the sample is exposed to the climatic chamber conditions simulating dynamic outdoor climate. The inner surface is exposed to a passive cell with fixed initial climate to simulate the indoor climate. The evolution of temperature and relative humidity at various locations, including $x = 3, 7.5, 12.5$ cm, as well as inner and outer surfaces, is recorded by

sensors. A schematic view of the experiment is shown in Fig. 2. Prior to any testing, the entire system, including climatic chamber, passive cell, and all studied specimens, must reach an initial equilibrium state at $T = 23°C$ and $RH = 50\%$. After that, the tests start by changing the outdoor climate according to a certain scenario. In this paper, two typical scenarios have been studied.

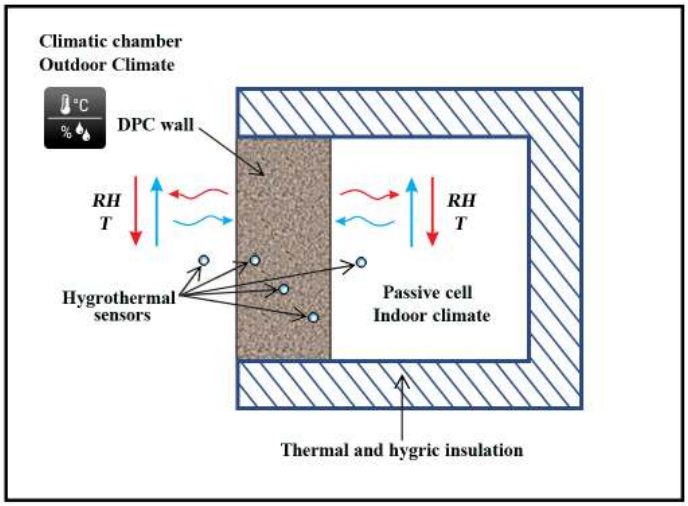

Figure 2: Schematic representation of the experiment. Refer to [43] for detailed experimental setup.

- The first one simulates the response of DPC wall to a sudden variation in relative humidity. The testing is performed at a stable outdoor temperature $T = 23°C$. The outdoor relative humidity increases to 75% and keeps constant for 9 days. Afterwards, the outdoor relative humidity decreases to 33% immediately, and this boundary condition is maintained for another 9 days. Fig. 3 presents the actual relative humidity profiles at outdoor and indoor ambiances which was obtained from experimental measurement and used as boundary conditions for calculations.

- The second one focuses on the performance of DPC wall to a repeated temperature cycles. In this case, the outdoor relative humidity is fixed at $RH = 50\%$. After an initial step change from $T = 23°C$ to $T = 40°C$, the system experiences a cyclic variation of the temperature, from $T = 40°C$ to $T = 23°C$, with a 12 h period. The duration of the entire testing is 4 days. The specific temperature boundary conditions are shown in Fig. 4

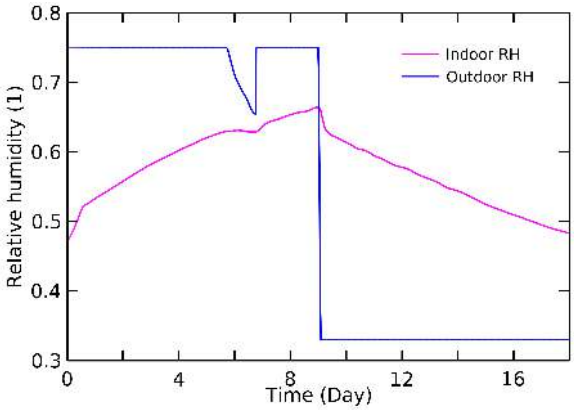

Figure 3: RH boundary conditions of scenario 1

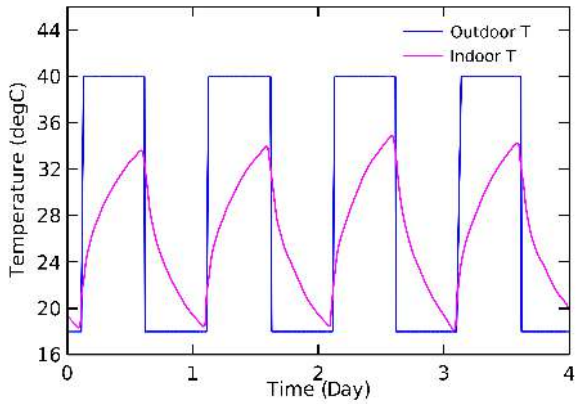

Figure 4: Temperature boundary conditions of scenario 2

3.2. Numerical Modelling method

For a quantitative solutions, the governing equations are discretised in space by finite elements using a Galerkin procedure and in time by backward Euler method. The relative humidity ϕ and temperature T are basic variables of the studied phenomenon. Vector notation is now introduced. These basic variables are expressed in the whole domain by global shape function matrices $\mathbf{N}^{\phi}$ and $\mathbf{N}^{T}$ as function of nodal value vectors $\mathbf{\Phi}$ and $\mathbf{T}$:

$$\phi = \phi(t) = \mathbf{N}^{\phi}\mathbf{\Phi}(t) \tag{30}$$

$$T = T(t) = \mathbf{N}^T \mathbf{T}(t) \tag{31}$$

The Galerkin method is employed to obtain a weak form of the governing equations. After substitution of defined basic variables into (14) and (20) and some transformations the following set of algebraic equations in space is obtained (see Appendix for details):

$$\mathbf{K_w}\mathbf{\Phi} + \mathbf{K_{WT}}\mathbf{T} + \mathbf{C_{WD}}\dot{\mathbf{\Phi}} = \mathbf{f_\Phi} \tag{32}$$

$$\mathbf{K_{TW}}\mathbf{\Phi} + \mathbf{K_T}\mathbf{T} + \mathbf{C_{TD}}\dot{\mathbf{\Phi}} + \mathbf{C_T}\dot{\mathbf{T}} = \mathbf{f_T} \tag{33}$$

Thereafter, an appropriate iterative time marching scheme is required to solve the transient coupled model of moisture transport and heat transfer. In this paper, Euler implicit scheme (backward Euler method) is adopted because of its high stability. The full discretisation in time allows the algebraic equations transforms into the following forms:

$$\mathbf{K_W}^{n+1}\mathbf{\Phi}^{n+1} + \mathbf{K_{WT}}^{n+1}\mathbf{T}^{n+1} + \mathbf{C_{WD}}^{n+1}\frac{\mathbf{\Phi}^{n+1} - \mathbf{\Phi}^n}{\delta t} = \mathbf{f_\Phi}^{n+1} \tag{34}$$

$$\mathbf{K_{TW}}^{n+1}\mathbf{\Phi}^{n+1} + \mathbf{K_T}^{n+1}\mathbf{T}^{n+1} + \mathbf{C_{TD}}^{n+1}\frac{\mathbf{\Phi}^{n+1} - \mathbf{\Phi}^n}{\delta t} + \mathbf{C_T}^{n+1}\frac{\mathbf{T}^{n+1} - \mathbf{T}^n}{\delta t} = \mathbf{f_T}^{n+1} \tag{35}$$

where superscript $n+1$ denotes that the system is written at time $t_{n+1} = t_n + \delta t_n$. δt_n is the time increment between two adjacent time points. The solution for the nonlinear system at time point t_{n+1} can be calculated based on the solution at previous time point t. In another words, for a given initial conditions $\mathbf{\Phi^0}$ and $\mathbf{T}^0$ at time $t = 0$, the solution of the nonlinear system $\left(\mathbf{\Phi}^{n+1}, \mathbf{T}^{n+1}\right)$ can be calculated for every time point $n = 0, \ldots, N-1$. The Newton-Raphson algorithm is used to solve the system.

As any transfer of heat and moisture towards the lateral surfaces is avoided, the system is assumed to follow one-dimensional hypothesis. The system is divided into 1500 uniform mesh elements on the whole length. The mesh size is big enough to optimize the computing time and fine enough to well follow the fields. Moreover, the time step is adaptive according to the convergence rate to obtain quantitative solutions of the governing equations efficiently.

To distinguish the contribution of dynamic capillarity effect and hysteresis on mass and heat transfer, a certain experiment is respectively simulated by three models including standard model, hysteresis model and dynamic hysteresis model. As for standard modelling, We employ the usual model that lacks dynamic terms for simulation. The simulations are implemented based on the average sorption curve. Concerning hysteresis modelling, only the hysteresis effect is included, while the potential contribution of dynamic effect is completely neglected. Since the sample was partially desiccated before the start of experiment, the intermediate adsorption-desorption curves begin from the main desorption curve in this case. Concerning dynamic hysteresis modelling, the dynamic model has been implemented with consideration of hysteresis model.

The moisture and heat exchange on the surface of porous media is determined by the interaction between porous media and the surrounding environment. The gradient, observed in the water vapour pressure and temperature in the vicinity of the open surfaces of porous media, governs the mass and heat transfer from the interior of the porous media to its open surfaces. The Neumann-type boundary condition is a feasible choice in this case:

$$Q_\Omega = h\left(T_\Omega - T_{amb}\right) \tag{36}$$

$$G_\Omega = \beta\left(P_{v,\Omega} - P_{v,amb}\right) \tag{37}$$

where Q_Ω and G_Ω are heat and mass fluxes at open surfaces, respectively. T_Ω and $P_{v,\Omega}$ are the temperature and water vapour pressure within the porous medium near open surfaces. T_{amb} and $P_{v,amb}$ are the external temperature and water vapour pressure in the ambient environment. The heat exchange coefficient h consists of the convective heat transfer coefficient h_c and the radiative heat transfer coefficient. In reality, the actual local coefficients on the exterior and interior surfaces may vary slightly. Despite this potential difference, we have neglected it for simplicity. The heat exchange coefficient is assumed to be 8 $\left(Wm^{-2}K^{-1}\right)$ for both the exterior and interior surfaces [21]. The moisture transfer coefficient at boundaries is set to $75 \times 10^{-9}\left(s/m\right)$ on the exterior surface and $25 \times 10^{-9}\left(s/m\right)$ on the interior surface [9].

For the purpose of implementing the dynamic model to simulate heat and moisture transfer for

the scenario 1, the contribution of dynamic effect should be identified. In general, the dynamic coefficient τ is formulated as a function of water saturation. Considerable attention has been paid to the dependency of this coefficient τ on water saturation or moisture content [22, 23, 44, 45]. However, there is no widely accepted formula to identify its value. Moreover, the time change rate of saturation $\partial S_w/\partial t$ varies significantly from the open surface to the interior. This variation can even reach several orders of magnitude. It indicates that the second-order term calculated by $\tau \frac{\partial S_w}{\partial t}$ is very sensitive to the dynamic coefficient τ. If τ is not perfectly identified, the dynamic capillary pressure P_c^{dyn} could be many times as larger as the equilibrium capillary pressure P_c. However, this is not the case in reality. Previous studies have indicated that the second order term induced by the dynamic effect is a supplement to capillary pressure rather than a predominate factor [22, 44, 46]. In addition, it can cause non-convergence issue in the FEM calculation.

In this paper, a deliberate method is put forward to ensure an appropriate dynamic capillary pressure and high rate of convergence in finite element analysis. No specific form of τ-S_w relationship is provided. But, the additional contribution caused by the dynamic effect on capillary pressure is defined as a function of capillary pressure P_c, spatial distribution coefficient $F(x)$ and time distribution coefficient $G(t)$, as presented below:

$$\tau \frac{\partial S_w}{\partial t} = F(x)\, G(t)\, P_c \tag{38}$$

First, $F(x)$ and $G(t)$ in Eq. (38) have been determined according to experimental tests. A higher RH gradient, resulting in faster change of relative humidity, leads to stronger dynamic effect. When a step change of external RH is imposed, the dynamic effect is supposed to start with highest performance and then become weak gradually as time goes by. Indeed, the dynamic model reproduces implicitly the fluid velocity effect. It is not neglected under high velocity instead of quasistatic behaviour. The closer the location is to the open surface, the more significant the local dynamic effect is assumed to be. These characteristics provide guidance for the definition of $F(x)$ and $G(t)$. In order to avoid overestimation of dynamic effect as mentioned previously, their absolute values are expected to be in the range of 0 to 1. The interpolation functions $F(x)$ and $G(t)$

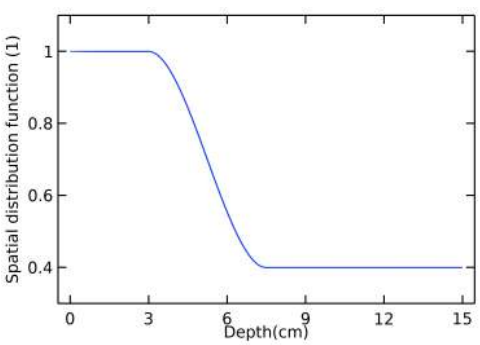

(a) Spatial distribution function $F(x)$

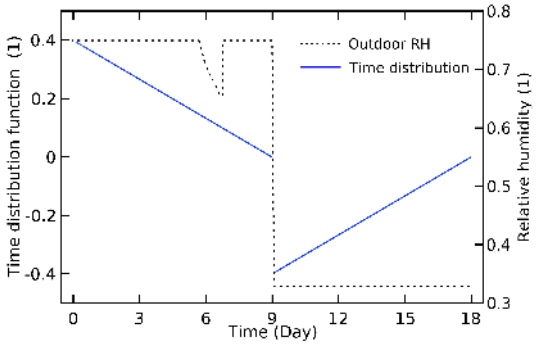

(b) Time distribution function $G(t)$

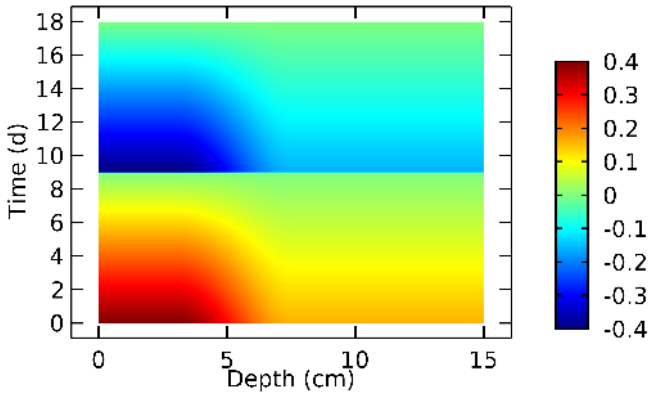

(c) Spatiotemporal evolution of coefficient for dynamic effect

Figure 5: Coefficient function used for calculation of additional capillary pressure caused by dynamic effect

are plotted in Fig. 5. They have been determined initially by providing the evolution of relative humidity to have relatively high agreement with corresponding experimental data. Note that the discontinuity in the function $G(t)$ corresponds to an abrupt change in RH. The dynamic effect coefficient is proportional to the drying or wetting rate. Indeed, the imposition of a new boundary condition differing from the initial condition on a system induces a maximum drying or wetting rate followed by a decrease over time until the new stable state is reached. This also explains why the absolute value of the function $G(t)$ keeps decreasing under stable boundary conditions. The specific spatiotemporal evolution of this coefficient is shown in Fig. 5 (c).

4. Results analysis and discussion

In this part, the simulation results obtained by three different models including standard, hysteresis and dynamic hysteresis models are presented and compared with the corresponding experimental data.

4.1. Scenario 1: Step change in RH at room temperature

4.1.1. Observations

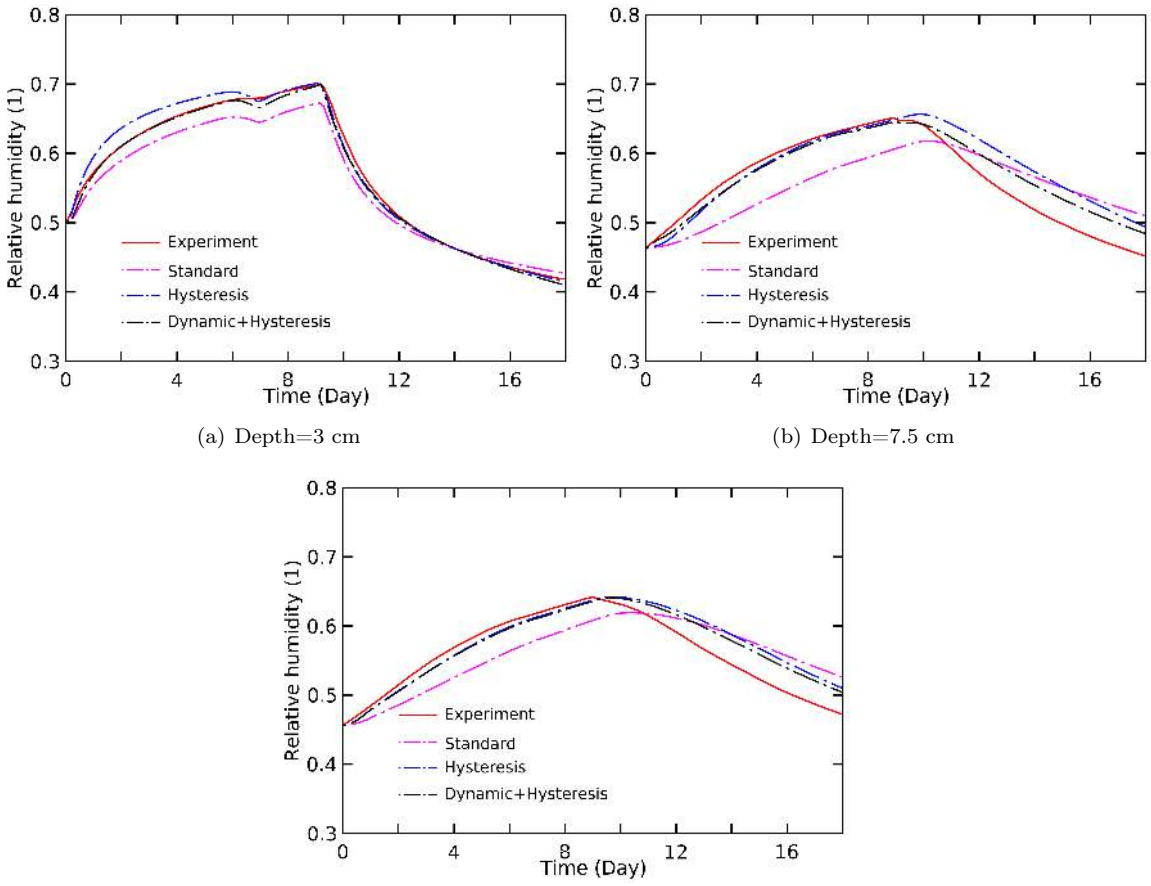

(a) Depth=3 cm

(b) Depth=7.5 cm

(c) Depth=12.5 cm

Figure 6: Comparison of relative humidity evolution obtained by dynamic hysteresis, hysteresis and standard modelling with experimental data at different depths.

Figure 6 presents the comparison between experimental data with numerical simulations obtained with standard, hysteresis and dynamic hysteresis models. The simulation results of relative humidity evolution are plotted for certain depth locations. More or less significant deviations between standard modelling results and experimental data are observed. The response of standard modelling to the step change in relative humidity seems to be less sensitive. Compared with experimental data, the standard modelling always underestimates the increment of relative humidity during adsorption stage and overestimates the decrement of relative humidity during desorption stage, which is in accordance with observations reported in [47].

The simulated evolution of relative humidity when considering hysteresis effect shows a huge gap with the numerical results of standard model. Even though the numerical result from hysteresis model shows a non-negligible discrepancy with corresponding experimental data, a significant improvement is achieved using average sorption curve. In particular, the modelling considering hysteresis effect accelerates the moisture transport which results in a higher relative humidity which is close to measured data at the location of depth 7.5 cm and 12.5 cm during the adsorption stage.

The dynamic hysteresis modelling gives quite good numerical results, especially at location close to outdoor surface with depths 3 cm. During desorption stage, the numerical results at depth of 7.5 cm and 12.5 cm display a slight gap with the corresponding experimental data. However, by reviewing the poor and average performance of standard and hysteresis models in the same figures respectively, the dynamic hysteresis modelling provides numerical results have the highest agreement with experimental data. During adsorption stage, dynamic effect seems to have a weak influence on hygric behaviour of DPC at depths of 7.5 cm and 12.5 cm, and in this case the use of hysteresis model yields satisfactory results. However, taking into account dynamic effect is important at the location close to outdoor surface where saturation in porous media experiences a relatively rapid change. Moreover, the dynamic hysteresis modelling also ameliorates the numerical results for desorption stage (see Fig. 6 (b-c)). It indicates that the dynamic effect also plays an important role in alleviating the underestimation on drying rate. The results comparisons of dynamic hysteresis modelling with hysteresis modelling reveal that the dynamic effect seems to be able to accelerate desorption and decelerate adsorption.

4.1.2. Discussion on RH evolution

This deviation varies with the location and reaches to maximum at depth 7.5 *cm*. The minimum gap is found at the location close to outdoor surface at depth 3 *cm*. Similar phenomena were also observed in previous literature [18]. One reasonable explanation for these obvious deviation is the negligence of hysteresis effect. If hysteresis is not considered, the retained water due to ink-bottle effect during wetting and drying cycles is neglected. The history of water content (intermediate sorption curve) must be mastered in order to provide a more accurate relationship between relative humidity and moisture content, which plays an important role in predicting moisture transport. As introduced previously, the DPC materials exhibit distinct characteristic of hysteresis.

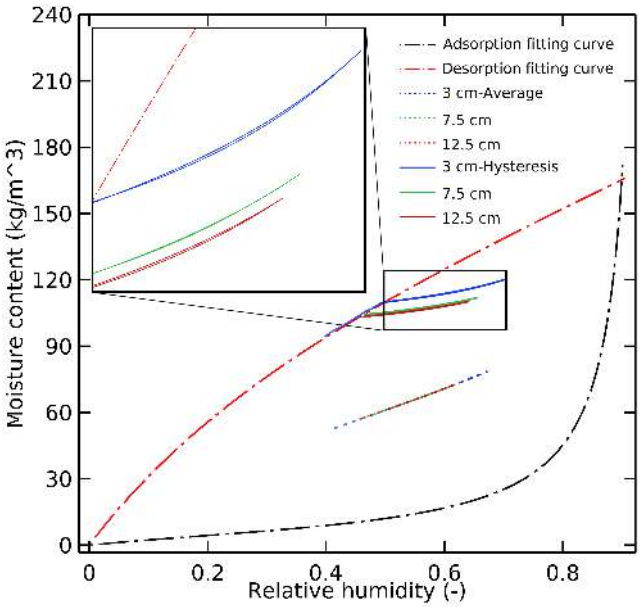

Figure 7: Comparison of hysteresis sorption curve with average sorption curve

Hysteresis and average sorption curves are plotted and compared in Fig. 7. There is a significant difference between these two kinds of sorption curves. The hysteresis sorption curves begin to generate from the main desorption curve due to the fact that the manufactured specimen suffers a partial drying before starting the test. A step increase in relative humidity imposed on the outdoor surface of the specimen induces an adsorption by following the wetting scannin curve. Thereafter,

because of the external relative humidity decreases to 0.33, the specimen begins to dry, following a new drying scanning curve. Indeed, the start point of this new drying scanning curve is the end point of the previous adsorption scanning curve. Afterwards, the main desorption curve will be used to take the place of drying scanning curve for the prediction of drying once the main desorption curve is reached. It is important to note that the Mualen II model enables the sorption curves to vary at different locations according to local moisture content state. Furthermore, there is no obvious difference between adsorption and desorption hysteresis curves. It indicates that the hysteresis effect seems to have a weak impact on hygric behaviour of this kind of porous material as the relative humidity ranges from 0.4 to 0.7. On the other hand, the average sorption curve is entirely independent of the history of moisture content, which results in an underestimation of the sorption curve. Because the hysteresis sorption curves, taking into account moisture content history, seem closer to the reality, the hysteresis model provides better results than standard model.

Even though the hysteresis model optimizes the simulation results, a non-negligible deviation still exists, especially at the location close to the open surface or when a high RH gradient is imposed. For instance, as observed in Fig. 6 (a), the hysteresis model overestimates the relative humidity at depth 3 cm during the adsorption stage; similar phenomena are observed at depths 7.5 cm and 12.5 cm when a high RH gradient exists during the desorption stage (Fig. 6 (b-c)). It indicates that the hysteresis model appears to have limitations. Indeed, a higher time change rate of saturation induced by step change of external relative humidity results in dynamic effect on capillary pressure, which has a potential influence on moisture transport [48, 49]. In order to accurately predict the evolution of relative humidity under conditions where a high RH gradient exists between the external environment and the specimen, both dynamic and hysteresis effects should be studied.

These results show that the model taking into account dynamic and hysteresis effects is apparently more appropriate than standard model and hysteresis model to simulate hygric behaviour of cement-based materials under repeated wetting and drying cycles. One important reason is that the dynamic hysteresis model not only takes into account dynamic capillarity effect when high RH gradient are imposed on specimen but also adopts hysteresis sorption curves based on moisture

content history.

The slight deviation between the dynamic hysteresis modelling curves and experimental results could be attributed to the dependence of the moisture transport coefficient on moisture content-relative humidity relationship. However, a constitutive relationship defined under steady-state condition is not suitable to transient transport process. Nonetheless, we strictly deal with the dynamic effect within capillary pressure and neglect possible dynamic effect in the moisture transport coefficient. In addition, the experimental test may be different from the idealized configuration of the dynamic hysteresis model, in which the system is supposed to be insulated on lateral surfaces. However, from the experimental point of view, it is difficult to ensure the one dimension moisture and heat transfers across the thickness of DPC wall, because the artificial insulation of enclosure is difficult to provide 100% protection against moisture and heat infiltration on lateral surfaces of the DPC wall. Likewise, before the beginning of experimental test, the initial condition of the DPC wall has been influenced by consecutive disturbances of outdoor relative humidity.

4.1.3. Discussion on temperature evolution

By retrospecting the governing model for moisture and heat transfer, there is a coupling between moisture transport and heat transfer. It indicates that the adsorption and desorption procedures caused by step change of external relative humidity are accompanied by temperature variation. The specific temperature evolutions at various depths of DPC wall are consistent with theoretical prediction and presented in Fig. 8.

The variations' amplitudes obtained by standard modelling are higher than the ones obtained from hysteresis and dynamic hysteresis modelling. Compared with the negligible contribution of dynamic phenomenon, the hysteresis phenomenon on heat transfer induced by moisture transport is more obvious but the absolute influence is still weak. Nevertheless, the temperature variation trends for the three modellings are similar at various depths. It can be noted that there is a sharp increase in temperature at the beginning of the simulation, even though the ambient temperature keeps constant at $T = 23°C$. Indeed, the condensation caused by adsorption is an exothermic physical procedure, which results in the temperature rise. Thereafter, the wall temperature de-

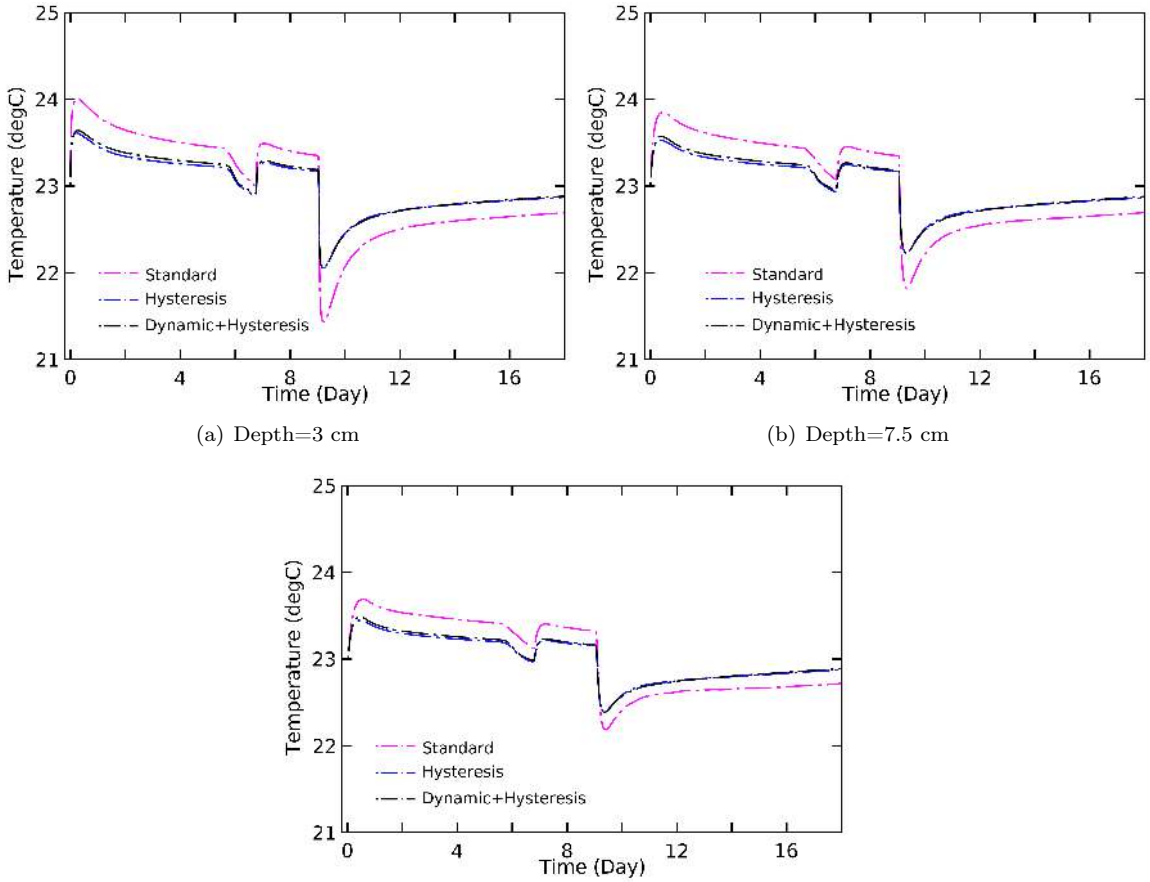

(a) Depth=3 cm

(b) Depth=7.5 cm

(c) Depth=12.5 cm

Figure 8: Comparisons of temperature curves simulated by dynamic hysteresis modelling with results of hysteresis modelling and standard modelling

creases gradually until the $9th$ day. Another step change of external RH from 75% to 33% at this moment leads to a sharp drop of wall temperature. A rational explanation behind the phenomenon is that the evaporation at the desorption stage is an endothermic procedure which results in wall temperature reduction. Following this instantaneous drop, the wall temperature begins to return to ambient temperature step by step. Similar phenomena are found in documented references [43, 50].

4.2. Scenario 2: Cyclic temperature variation

In this scenario, the thermal behaviour of DPC wall was studied. The DPC sample is subjected to outdoor cyclic temperature variations at constant ambient relative humidity condition $RH = 50\%$. The repeated variation consists of four successive cycles of $23°C - 40°C$. Each temperature is imposed for 12 h period and the duration of the entire test is 4 days. It means that tests are carried out in steady state of relative humidity. Three models including standard, hysteresis, dynamic hysteresis models are adopted to reproduce the temperature variation at depth 3 cm, 7.5 cm and 12.5 cm (Fig. 9 (a-c)). A simple but appropriate dynamic terms $\tau \frac{\partial S_w}{\partial t} = 0.3 P_c$ was used to ensure the potential contribution of dynamic capillarity effect on the system.

In general, the numerical results simulated by these three models are in good agreement with experimental curves. Differences between numerical and experimental results decrease closer to the indoor surface. The best overall agreement is observed at a depth of 12.5 cm. Nevertheless, the magnitudes of temperature evolution are slightly higher than experimental measurements. Analogous to the analysis in scenario 1, the inconsistency between experimental reality and idealized configuration of numerical simulation could contribute to justifying such discrepancy.

By comparing the three modelling curves with each other, similar thermal behaviour is observed at corresponding depths, especially at the locations 7.5 and 12.5cm. Only slight gap is observed between standard and hysteresis modelling at a depth of 3 cm. It indicates that the hysteresis effect seems to have weak influence on heat transfer in steady state of relative humidity. Likewise, even though a strong dynamic capillarity effect with $\tau \frac{\partial S_w}{\partial t} = 0.3 P_c$ is used in the dynamic hysteresis modelling, numerical results are almost identical with the dynamic hysteresis model as with the hysteresis model. It suggests that dynamic capillarity is negligible in this case. After the discussion above, it can be concluded that neither the hysteresis effect nor the dynamic capillarity effect plays an important role in heat transfer. This is expected because thermal behaviour is greatly dependent on heat conduction rather than moisture transport. Therefore, the additional contribution of dynamic and hysteresis on moisture transport has weaker influence on heat transfer.

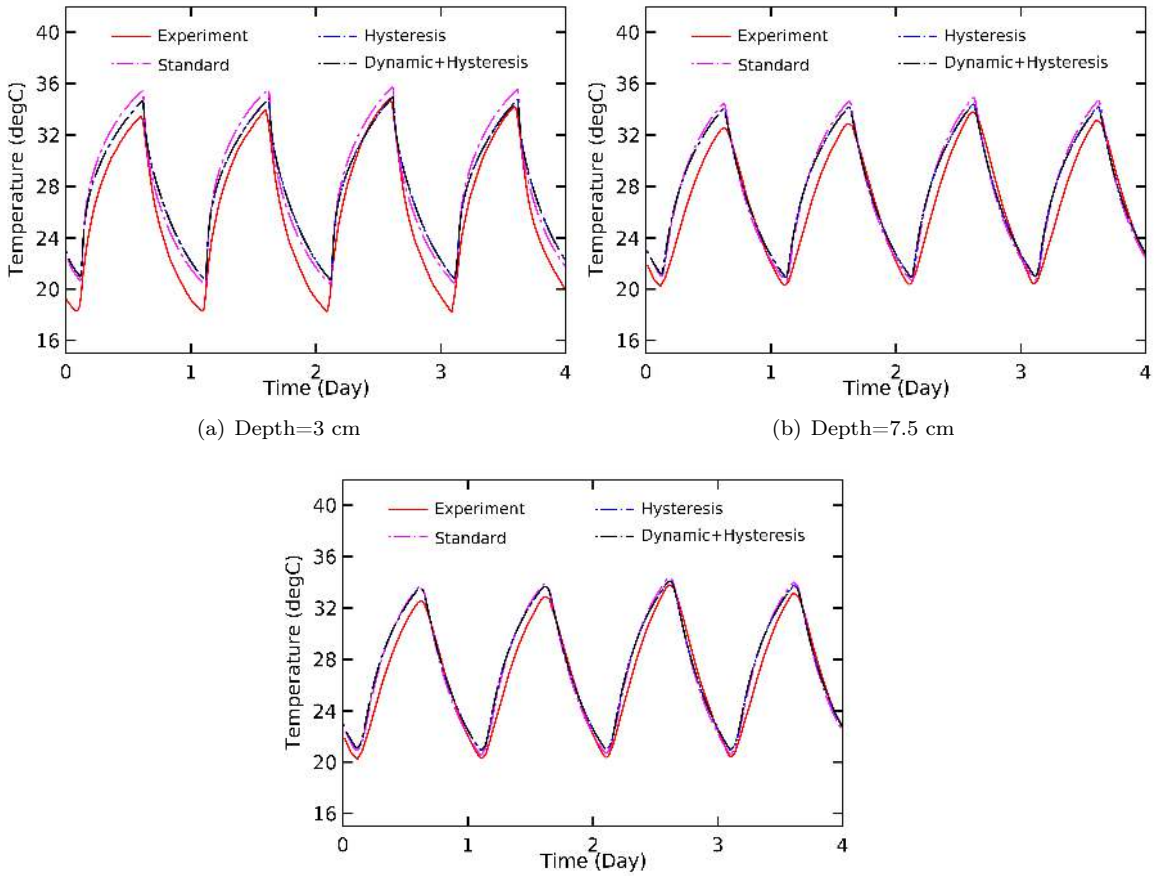

(a) Depth=3 cm

(b) Depth=7.5 cm

(c) Depth=12.5 cm

Figure 9: Comparison of temperature evolution obtained by dynamic hysteresis, hysteresis and standard modelling with experimental data at different depths

5. Conclusion and perspective

This work has introduced a more advanced model that significantly enhances the ability to predict heat and moisture transfer in porous building materials by accounting for the intricate interplay of moisture hysteresis effect and dynamic capillarity effect. This dynamic hysteresis model has a higher performance in the prediction of the hygrothermal behaviour of bio-based building materials when compared to standard models. As a practical outcome, this model provides a valuable tool for designing superior materials and optimizing their applications, ultimately promoting the efficiency

and sustainability of bio-based building constructions. The following conclusions can be drawn:

- Compared to the standard model, the hysteresis model, based on the assumption of local thermodynamic equilibrium and incompressible fluids, is more advanced as the hysteresis phenomenon between adsorption and desorption procedures as well as the moisture content history has been considered. Because hysteresis sorption curves provide a more accurate constitutive relationship between moisture content and relative humidity, the hysteresis model gives better results than the standard model, especially for predicting relative humidity evolution. However, the hysteresis model seems to be limited when a high RH gradient is imposed.

- The dynamic hysteresis model is more complete than hysteresis model, because potential contribution of dynamic effect on moisture transport and heat transfer is included. Comparisons presented in this paper highlight that the dynamic hysteresis model shows the evolution of RH having the highest agreement with experimental data. It confirms the validity of the dynamic hysteresis model. Thus, not only moisture hysteresis effect but also dynamic capillarity effect should be emphasized in the prediction of relative humidity evolution under the condition that the moisture content experiences rapid variation.

- The adsorption and desorption phenomena are accompanied by temperature variation due to the coupling between moisture transport and heat transfer. Numerical results demonstrate that the absolute impact of moisture transport on heat variation is not significant but causes a sensitive response. In addition, a negligible contribution of dynamic effect shows that the hysteresis effect on temperature variation, induced by adsorption or desorption, is relatively stronger, but the absolute influence is still weak.

- The response of the DPC wall to a repeated temperature cycles simulated by these three models is similar and in good agreement with experimental measurements. It reveals that neither dynamic effect nor hysteresis effect has significant influence on heat transfer in this case. Thus, if heat transfer is greatly dependent on heat conduction, the standard model is recommended for predicting temperature variation.

Although we have made efforts to improve the simulation results, we acknowledge that there have been slight deviations between our model predictions and the corresponding experimental measurements. We attribute these deviations to potential factors such as the inconsistency between experimental reality and the idealized configuration used in our numerical simulations.

For the prospective, to establish the credibility and potential of our model, it is crucial to validate its predictions by comparing them with data from other sources or experimental data in future work. By incorporating additional validation studies, we can assess the model's performance and ensure its robustness across different scenarios. As the pore network and fluid properties would be affected by temperature variation, which leads to a variation of sorption curves, further improvement could be made by taking into account this variation for dynamic hysteresis model. In addition, it is crucial to pursue further quantification of the dynamic effect coefficient, with a specific focus on mitigating the inherent uncertainties associated with quantifying the dynamic capillarity effect.

6. Appendix

The derivation of discrete form of governing Eqs. (14) and (20) and the full expression of the matrices in the discrete Eqs. (32) and (33) are shown here in detail.

The dynamic models for moisture transport Eq. (14) and heat transfer Eq. (20) after modification are rewritten in the following form:

$$\xi_\phi \dot{\phi} - \nabla \cdot \left[C_{\phi,1} \nabla \left(\xi_{dyn} \dot{\phi} \right) \right] + \nabla \cdot \left(D_{\phi,1} \nabla \phi \right) + \nabla \cdot \left(D_{\phi,2} \nabla T \right) = 0 \tag{39}$$

$$\xi_T \dot{T} - \nabla \cdot (\lambda \nabla T) - h_{lv} \nabla \cdot \left(C_{T,1} \nabla \left(\xi_{dyn} \dot{\phi} \right) \right) + h_{lv} \nabla \cdot \left(D_{T,1} \nabla \phi \right) + h_{lv} \nabla \cdot \left(D_{T,2} \nabla T \right) = 0 \tag{40}$$

where

$$C_{\phi,1} = K + \delta_p \phi P_v^{sat}(T) \frac{M_w \beta}{\rho_w RT} \tag{41}$$

$$D_{\phi,1} = K \frac{\partial P_c}{\partial w} \frac{\partial w}{\partial \phi} - \delta_p \beta P_v^{sat}(T) \tag{42}$$

$$D_{\phi,2} = D_{T,2} = \delta_p \phi P_v^{sat}(T) \frac{\xi_{dyn} \dot{\phi} M_w \beta}{\rho_w RT^2} - \delta_p \phi \beta \frac{\partial P_v^{sat}(T)}{\partial T} \tag{43}$$

$$C_{T,1} = \frac{\delta_p \phi P_v^{sat}(T) M_w \beta}{\rho_w RT} \tag{44}$$

$$D_{T,1} = -\delta_p \beta P_v^{sat}(T) \tag{45}$$

The interpolating functions $\phi = \mathbf{N}^{\phi} \mathbf{\Phi}(t)$ and $T = \mathbf{N}^{T} \mathbf{T}(t)$ are introduced to approximate the dependent variables ϕ and T. By using the Galerkin weighted residual method and setting the integral of the residual function equal to zero, the moisture transport and heat transfer governing equations are transformed into:

$$\int_{\Omega} \mathbf{N}^{\phi,\mathrm{T}} \cdot \left\{ \xi_{\phi} \dot{\phi} - \nabla \cdot \left[C_{\phi,1} \nabla \left(\xi_{dyn} \dot{\phi} \right) \right] + \nabla \cdot \left(D_{\phi,1} \nabla \phi \right) + \nabla \cdot \left(D_{\phi,2} \nabla T \right) \right\} d\Omega = 0 \tag{46}$$

$$\int_{\Omega} \mathbf{N}^{T,\mathrm{T}} \cdot \left\{ \begin{array}{l} \xi_T \dot{T} - \nabla \cdot (\lambda \nabla T) - h_{lv} \nabla \cdot \left[C_{T,1} \nabla \left(\xi_{dyn} \dot{\phi} \right) \right] \\ + h_{lv} \nabla \cdot \left(D_{T,1} \nabla \phi \right) + h_{lv} \nabla \cdot \left(D_{T,2} \nabla T \right) \end{array} \right\} d\Omega = 0 \tag{47}$$

where $\mathbf{N}^{\phi,\mathrm{T}}$ and $\mathbf{N}^{T,\mathrm{T}}$ are transpose of $\mathbf{N}^{\phi}$ and $\mathbf{N}^{T}$. After applying the Green's theorem to replace the second derivative terms in above equations and replacing the dependent variables ϕ and T by using corresponding interpolating functions Eqs. (30) and (31), the weak forms of moisture

transport and heat transfer models are given as below:

$$\begin{aligned}
&-\int_{\Omega}\nabla\mathbf{N}^{\phi,\mathrm{T}}\cdot D_{\phi,1}\nabla\mathbf{N}^{\phi}d\Omega\mathbf{\Phi}-\int_{\Omega}\nabla\mathbf{N}^{\phi,\mathrm{T}}\cdot D_{\phi,2}\nabla\mathbf{N}^{T}d\Omega\mathbf{T}\\
&+\int_{\Omega}\nabla\mathbf{N}^{\phi,\mathrm{T}}\cdot C_{\phi,1}\nabla\left(\xi_{dyn}\mathbf{N}^{\phi}\right)+\mathbf{N}^{\phi,\mathrm{T}}\cdot\xi_{\phi}\mathbf{N}^{\phi}d\Omega\dot{\mathbf{\Phi}}\\
&=\int_{\Gamma_{\phi}}\mathbf{N}^{\phi,\mathrm{T}}\left(C_{\phi,1}\nabla\left(\xi_{dyn}\dot{\phi}\right)-D_{\phi,1}\nabla\phi-D_{\phi,2}\nabla T\right)\cdot\mathbf{n}d\Gamma
\end{aligned}\tag{48}$$

$$\begin{aligned}
&-\int_{\Omega}\nabla\left(\mathbf{N}^{T,\mathrm{T}}h_{lv}\right)\cdot D_{T,1}\nabla\mathbf{N}^{\phi}d\Omega\mathbf{\Phi}+\int_{\Omega}\nabla\mathbf{N}^{T,\mathrm{T}}\cdot\lambda\nabla\mathbf{N}^{T}-\nabla\left(\mathbf{N}^{T,\mathrm{T}}h_{lv}\right)\cdot D_{T,2}\nabla\mathbf{N}^{T}d\Omega\mathbf{T}\\
&+\int_{\Omega}\nabla\left(\mathbf{N}^{T,\mathrm{T}}h_{lv}\right)\cdot C_{T,1}\nabla\left(\xi_{dyn}\mathbf{N}^{\phi}\right)d\Omega\dot{\mathbf{\Phi}}+\int_{\Omega}\mathbf{N}^{T,\mathrm{T}}\cdot\xi_{T}\mathbf{N}^{T}d\Omega\dot{\mathbf{T}}\\
&=\int_{\Gamma_{T}}\mathbf{N}^{T,\mathrm{T}}\left(\lambda\nabla T+h_{lv}C_{T,1}\nabla\left(\xi_{dyn}\dot{\phi}\right)-h_{lv}D_{T,1}\nabla\phi-h_{lv}D_{T,2}\nabla T\right)\cdot\mathbf{n}d\Gamma
\end{aligned}\tag{49}$$

The terms on the right hand sides of Eqs. (48) and (49) indicate boundary flux of moisture and heat, respectively. $\mathbf{n}$ is the outward unit normal vector to the boundary surface. Therefore, the algebraic form of moisture transport model (32) in space is obtained if the following definitions are

used:

$$\mathbf{K_W} = -\int_{\Omega} \nabla \mathbf{N}^{\phi,\mathrm{T}} \cdot D_1 \nabla \mathbf{N}^{\phi} d\Omega \tag{50}$$

$$\mathbf{K_{WT}} = -\int_{\Omega} \nabla \mathbf{N}^{\phi,\mathrm{T}} \cdot D_2 \nabla \mathbf{N}^{T} \tag{51}$$

$$\mathbf{C_{WD}} = \int_{\Omega} \nabla \mathbf{N}^{\phi,\mathrm{T}} \cdot C_1 \nabla \left(\xi_{dyn} \mathbf{N}^{\phi} \right) + \mathbf{N}^{\phi,\mathrm{T}} \cdot \xi_{\phi} \mathbf{N}^{\phi} d\Omega \tag{52}$$

$$\mathbf{f_{\Phi}} = \int_{\Gamma_{\phi}} \mathbf{N}^{\phi,\mathrm{T}} \left(C_1 \nabla \left(\xi_{dyn} \dot{\phi} \right) - D_1 \nabla \phi - D_2 \nabla T \right) \cdot \mathbf{n} d\Gamma \tag{53}$$

Meanwhile, the appropriate matrices comprising the coefficients implicit for algebraic form of heat transfer model are gathered as follows:

$$\mathbf{K_{TW}} = -\int_{\Omega} \nabla \left(\mathbf{N}^{T,\mathrm{T}} h_{lv} \right) \cdot D_{T,1} \nabla \mathbf{N}^{\phi} d\Omega \tag{54}$$

$$\mathbf{K_T} = \int_{\Omega} \nabla \mathbf{N}^{T,\mathrm{T}} \cdot \lambda \nabla \mathbf{N}^{T} - \nabla \left(\mathbf{N}^{T,\mathrm{T}} h_{lv} \right) \cdot D_{T,2} \nabla \mathbf{N}^{T} d\Omega \mathbf{T} \tag{55}$$

$$\mathbf{C_{TD}} = \int_{\Omega} \nabla \left(\mathbf{N}^{T,\mathrm{T}} h_{lv} \right) \cdot C_{T,1} \nabla \left(\xi_{dyn} \mathbf{N}^{\phi} \right) d\Omega \tag{56}$$

$$\mathbf{C_T} = \int_{\Omega} \mathbf{N}^{T,\mathrm{T}} \cdot \xi_T \mathbf{N}^{T} d\Omega \tag{57}$$

$$\mathbf{f_T} = \int_{\Gamma_T} \mathbf{N}^{T,\mathrm{T}} \left(\lambda \nabla T + h_{lv} C_{T,1} \nabla \left(\xi_{dyn} \dot{\phi} \right) - h_{lv} D_{T,1} \nabla \phi - h_{lv} D_{T,2} \nabla T \right) \cdot \mathbf{n} d\Gamma \tag{58}$$

Acknowledgments

Authors would like to thank Charier-Edycem for the financial support. Also the National Centre for Scientific Research (CNRS) is acknowledged for the financial support of the international PRC project RATIC under the grant number 290993 and Natural Science Basic Research Plan in Shaanxi Province of China (grant No.2022JQ-483)

References

[1] H. J. Moon, S. H. Ryu, J. T. Kim, The effect of moisture transportation on energy efficiency and iaq in residential buildings, Energy and Buildings 75 (2014) 439–446.

[2] M. Woloszyn, T. Kalamees, M. O. Abadie, M. Steeman, A. S. Kalagasidis, The effect of combining a relative-humidity-sensitive ventilation system with the moisture-buffering capacity of materials on indoor climate and energy efficiency of buildings, Building and Environment 44 (2009) 515–524.

[3] O. F. Osanyintola, C. J. Simonson, Moisture buffering capacity of hygroscopic building materials: Experimental facilities and energy impact, Energy and Buildings 38 (2006) 1270–1282.

[4] J. Philip, D. De Vries, Moisture movement in porous materials under temperature gradients, Eos, Transactions American Geophysical Union 38 (1957) 222–232.

[5] A. Luikov, Application of irreversible thermodynamics methods to investigation of heat and mass transfer, International Journal of Heat and Mass Transfer 9 (1966) 139–152.

[6] X. Liu, Y. Chen, H. Ge, P. Fazio, G. Chen, Numerical investigation for thermal performance of exterior walls of residential buildings with moisture transfer in hot summer and cold winter zone of china, Energy and Buildings 93 (2015) 259–268.

[7] C. R. Pedersen, Combined heat and moisture transfer in building constructions, volume 214, Thermal Insulation Laboratory, Technical University of Denmark, 1990.

[8] I. Budaiwi, R. El-Diasty, A. Abdou, Modelling of moisture and thermal transient behaviour of multi-layer non-cavity walls, Building and Environment 34 (1999) 537–551.

[9] H. M. Künzel, Simultaneous heat and moisture transport in building components, One-and two-dimensional calculation using simple parameters. IRB-Verlag Stuttgart 65 (1995).

[10] H. Janssen, B. Blocken, J. Carmeliet, Conservative modelling of the moisture and heat transfer in building components under atmospheric excitation, International Journal of Heat and Mass Transfer 50 (2007) 1128–1140.

[11] M. Rahim, A. T. Le, O. Douzane, G. Promis, T. Langlet, Numerical investigation of the effect of non-isotherme sorption characteristics on hygrothermal behavior of two bio-based building walls, Journal of Building Engineering 7 (2016) 263–272.

[12] K. Abahri, R. Belarbi, A. Trabelsi, Contribution to analytical and numerical study of combined heat and moisture transfers in porous building materials, Building and Environment 46 (2011) 1354–1360.

[13] C. Maalouf, A. T. Le, S. Umurigirwa, M. Lachi, O. Douzane, Study of hygrothermal behaviour of a hemp concrete building envelope under summer conditions in france, Energy and buildings 77 (2014) 48–57.

[14] F. Tariku, K. Kumaran, P. Fazio, Transient model for coupled heat, air and moisture transfer through multilayered porous media, International journal of heat and mass transfer 53 (2010) 3035–3044.

[15] W. Dong, Y. Chen, Y. Bao, A. Fang, A validation of dynamic hygrothermal model with coupled heat and moisture transfer in porous building materials and envelopes, Journal of Building Engineering 32 (2020) 101484.

[16] V. Baroghel-Bouny, Water vapour sorption experiments on hardened cementitious materials: Part i: Essential tool for analysis of hygral behaviour and its relation to pore structure, Cement and Concrete Research 37 (2007) 414–437.

[17] G. Promis, O. Douzane, A. T. Le, T. Langlet, Moisture hysteresis influence on mass transfer through bio-based building materials in dynamic state, Energy and Buildings 166 (2018) 450–459.

[18] D. Lelievre, T. Colinart, P. Glouannec, Hygrothermal behavior of bio-based building materials including hysteresis effects: Experimental and numerical analyses, Energy and Buildings 84 (2014) 617–627.

[19] N. Chennouf, B. Agoudjil, A. Boudenne, K. Benzarti, F. Bouras, Hygrothermal characterization of a new bio-based construction material: Concrete reinforced with date palm fibers, Construction and Building Materials 192 (2018) 348–356.

[20] M.-H. Benzaama, L. Rajaoarisoa, F. Boukhelf, Y. El Mendili, Hygrothermal transfer modelling through a bio-based building material: Validation of a switching-linear model, Journal of Building Engineering 55 (2022) 104691.

[21] T. Alioua, B. Agoudjil, N. Chennouf, A. Boudenne, K. Benzarti, Investigation on heat and moisture transfer in bio-based building wall with consideration of the hysteresis effect, Building and Environment 163 (2019) 106333.

[22] L. Zhuang, S. M. Hassanizadeh, C. Z. Qin, A. de Waal, Experimental investigation of hysteretic dynamic capillarity effect in unsaturated flow, Water Resources Research 53 (2017) 9078–9088.

[23] M. B. Janetti, H. Janssen, Impact of the drying rate on the moisture retention curve of porous building materials, Construction and Building Materials 258 (2020) 119451.

[24] H. W. Brown, Capillary pressure investigations, Journal of Petroleum Technology 3 (1951) 67–74.

[25] S. M. Hassanizadeh, W. G. Gray, Thermodynamic basis of capillary pressure in porous media, Water Resources Research 29 (1993) 3389–3405.

[26] S. M. Hassanizadeh, Advanced theories of two-phase flow in porous media, Handbook of porous media (2015) 47–62.

[27] S. P. Friedman, Dynamic contact angle explanation of flow rate-dependent saturation-pressure relationships during transient liquid flow in unsaturated porous media, Journal of adhesion science and technology 13 (1999) 1495–1518.

[28] D. Weitz, J. Stokes, R. Ball, A. Kushnick, Dynamic capillary pressure in porous media: Origin of the viscous-fingering length scale, Physical review letters 59 (1987) 2967.

[29] D. Wildenschild, J. Hopmans, J. Simunek, Flow rate dependence of soil hydraulic characteristics, Soil Science Society of America Journal 65 (2001) 35–48.

[30] D. Wildenschild, J. Hopmans, M. Rivers, A. Kent, Quantitative analysis of flow processes in a sand using synchrotron-based x-ray microtomography, Vadose Zone Journal 4 (2005) 112–126.

[31] H. K. Dahle, M. A. Celia, S. M. Hassanizadeh, Bundle-of-tubes model for calculating dynamic effects in the capillary-pressure-saturation relationship, Transport in Porous media 58 (2005) 5–22.

[32] A. Bourgeat, M. Panfilov, Effective two-phase flow through highly heterogeneous porous media: Capillary nonequilibrium effects, Computational Geosciences 2 (1998) 191–215.

[33] Z. Zhang, M. Thiery, V. Baroghel-Bouny, Investigation of moisture transport properties of cementitious materials, Cement and Concrete Research 89 (2016) 257–268.

[34] M. Mainguy, O. Coussy, V. Baroghel-Bouny, Role of air pressure in drying of weakly permeable materials, Journal of Engineering Mechanics 127 (2001) 582–592.

[35] J. Monteith, M. Unsworth, Principles of environmental physics: plants, animals, and the atmosphere, Academic Press, 2013.

[36] N. Benmansour, B. Agoudjil, A. Gherabli, A. Kareche, A. Boudenne, Thermal and mechanical performance of natural mortar reinforced with date palm fibers for use as insulating materials in building, Energy and Buildings 81 (2014) 98–104.

[37] Z. Zhong, Combined heat and moisture transport modeling for residential buildings, Ph.D. thesis, Purdue University, 2008.

[38] H. Derluyn, D. Derome, J. Carmeliet, E. Stora, R. Barbarulo, Hysteretic moisture behavior of concrete: Modeling and analysis, Cement and Concrete Research 42 (2012) 1379–1388.

[39] S. Merakeb, F. Dubois, C. Petit, Modeling of the sorption hysteresis for wood, Wood science and technology 43 (2009) 575.

[40] Y. Mualem, A conceptual model of hysteresis, Water Resources Research 10 (1974) 514–520.

[41] Y. Mualem, Modified approach to capillary hysteresis based on a similarity hypothesis, Water Resources Research 9 (1973) 1324–1331.

[42] Y. Mualem, A new model for predicting the hydraulic conductivity of unsaturated porous media, Water resources research 12 (1976) 513–522.

[43] N. Chennouf, B. Agoudjil, T. Alioua, A. Boudenne, K. Benzarti, Experimental investigation on hygrothermal performance of a bio-based wall made of cement mortar filled with date palm fibers, Energy and buildings 202 (2019) 109413.

[44] T. Sakaki, D. M. O'Carroll, T. H. Illangasekare, Direct quantification of dynamic effects in capillary pressure for drainage–wetting cycles, Vadose Zone Journal 9 (2010) 424–437.

[45] G. Camps-Roach, D. M. O'Carroll, T. A. Newson, T. Sakaki, T. H. Illangasekare, Experimental investigation of dynamic effects in capillary pressure: Grain size dependency and upscaling, Water Resources Research 46 (2010).

[46] Y. Zou, M. Saad, F. Grondin, Numerical investigation for the effect of deformation and dynamic pressure on the fast drainage of porous materials, European Journal of Environmental and Civil Engineering 26 (2022) 6605–6624.

[47] B. Moujalled, Y. A. Oumeziane, S. Moissette, M. Bart, C. Lanos, D. Samri, Experimental and numerical evaluation of the hygrothermal performance of a hemp lime concrete building: A long term case study, Building and Environment 136 (2018) 11–27.

[48] Y. Zou, M. Saad, F. Grondin, Contribution of the capillary pressure second-order term on fast drying of cement-based materials, Construction and Building Materials 296 (2021) 123422.

[49] Y. Zou, Modelling of the dynamic effects in capillary pressure in coupling with deformation on the desiccation of porous materials, Ph.D. thesis, École centrale de Nantes, 2020.

[50] M. Rahim, O. Douzane, A. T. Le, G. Promis, T. Langlet, Experimental investigation of hygrothermal behavior of two bio-based building envelopes, Energy and Buildings 139 (2017) 608–615.